3D printing of fully cellulose-based hydrogels by digital light processing

3D printing of fully cellulose-based hydrogels by Digital Light Processing

Abstract

We report on the development of natural-based, composite hydrogel inks for Digital Light Processing (DLP) 3D printing, composed entirely of cellulose-based-materials. DLP, which enables the production of complex constructs by photopolymerization, is already considered an environmentally friendly production method but it is still based on fossil chemicals, which may be a limit in the future. On the contrary, in view of a more environmental-friendly production, the development of natural inks will represent a further step to its wide-scale adoption. Here acrylated-carboxymethyl cellulose (mCMC) hydrogels are reinforced by the addition of biowastes-sourced cellulose nanocrystals (NCs) derived from oil palm empty fruit bunch, both pristine and functionalized, to produce hybrid polymeric networks.
It is demonstrated that the addition of such fillers does not affect the photocuring properties of the formulations while improving their printability through improvement in the mechanical properties, even with high content of water (97wt%). Furthermore, the printable hydrogels present intriguing characteristics such as controlled swelling and pH sensitivity. The use of fully-natural derived material with designed properties and complex geometries can open further perspectives in many fields, such as sensors, biomedical and soft robotics.

Introduction

3D printing has emerged as a ground-breaking tool to manufacture three-dimensional constructs, starting from a digital file (e.g. a CAD file) to fabricate nearly-net shape objects. Components can now be obtained with geometries not achievable with standard subtractive technologies, saving at the same time, material and energy [1,2]. Such characteristics lead to considering 3D printing as a key-enabling technology for sustainable production. Today, many application fields (electronics[1,2] biomedical[3,4], automotive[5], food [6,7] and fashion[8] industries) have embraced 3D printing technologies, due to high accuracy, rapid prototyping and the chance to create complex and customizable products.

Among the various 3D printing techniques, vat photopolymerization (VP) processes, such as stereolithography (SLA) and digital light processing (DLP), have gained a significant interest as a result of high resolution and fabrication speed[9]. Currently most of the commercially available inks for these technologies are based on acrylic and epoxy resins, derived from fossil sources. Such formulations are mainly based on previous ones from coatings industry, developed to achieve high polymerization rates, high accuracy and high resolution in printed structures. On the other hand, in view of a sustainable development, the use of synthetic chemicals is a drawback that may affect the potential of light based 3D printing technologies. The development of alternative eco-sustainable inks for VP-3D printing is a thus necessary step forward. In recent years, scientists have made a large effort to optimize natural materials for VP 3D printing, developing an increasing number of bio-derived inks [9] both for the production of highly reactive and mechanically stiff polymers [10–15] or for the development of 3D shaped hydrogels [16–21] which could find a great interest in the biomedical field. This work lies in this line, developing new 3D printable water-based ink composed only by cellulose derivate for the production of 3D hydrogels.

Cellulose is the most abundant natural polymer on Earth, [22][23]. As an available, biocompatible, biodegradable, versatile and mechanically efficient material[24], cellulose is largely used[25–29], both as raw material in the form of fibers/fibrils and, after modification, in the form of its water soluble derivatives. One of the most employed cellulose derivative is carboxymethyl-cellulose (CMC), a water-soluble cellulose ether, obtained by partial substitution of 2, 3, and 6 hydroxyl groups with carboxymethyl moieties[30]. CMC is affordable, biocompatible, biodegradable and FDA-approved[31,32]. It can also boast pH sensitivity, good water solubility, a fine three dimensional network and ease of chemical modifications[32–34]. Consequently, CMC is an ideal material to be used to 3D print hydrogels[20,32,35].

Hydrogels are cross-linked, polymeric networks, able to swell in water whilst retaining their shape and integrity[36]. They are largely used in many applications and especially in the biomedical field[37]. However, hydrogels cannot be shaped with conventional subtractive technologies due to their poor mechanical properties, so 3D printing is particularly interesting for these materials in order to fabricate components with complex geometry. Many natural polymers are currently used for the production of hydrogels, being advantageous in terms of recyclability and biodegradability[32]; in addition, they show some interesting properties (biocompatibility, low immunogenicity, cytocompatibility, versatility)[34] that can broaden their use in multiple applications.

Nevertheless, compared to standard synthetic counterparts, natural hydrogels show lower mechanical properties[35], making them less desirable for commercial applications. Furthermore, this lack of mechanical performance may affect the integrity of the 3D-printed parts, decreasing also the printing precision. A suitable strategy to improve mechanical properties involves the use of fillers, producing composite hydrogels. Literature in this field is huge [37–39], limiting to 3D printing, the most common fillers for hydrogels are carbon nanotubes and nanofibers[40–42], nanoclay[43,44], nanosilicates [45–47], graphene[48,49] and cellulose nanocrystals (NCs)[50–52].
The latter have attracted a tremendous interest [45,46] since those combine the aforementioned properties of cellulose with the advantages of nanostructured materials: high specific surface area, reactive surface functionalities and excellent strength and stiffness [53]. Cellulose nanocrystals (NCs) are highly crystalline nanorods with a width of 5-20 nm and length ranging from 100 nm to 500 nm[54]. They are usually extracted from various sources (wood, plants or biowaste) by H_2SO_4 hydrolysis, which provides the NCs surface with a negative charge, preventing the aggregation caused by the abundance of -OH groups [53,54]. Hydrogels embedding NCs have been already 3D printed employing different techniques: vat printing[40,55,56], DIW[57–59] and bioplotting [60–62].

Gathering all the aspects above mentioned, we developed methacrylated carboxymethyl cellulose (mCMC) hydrogels reinforced with NCs extracted from oil palm empty fruit bunches (EFB). The production of palm oil raised several disputes, related to deforestation, soil and workers exploitation and sustainability, nevertheless Indonesia and Malaysia are nowadays the largest producers of palm oil, so for these country this is an economic reality, even if with several criticism.[63,64] Considering the environmental effect of the oil palm plantation, it should be noted that it is a perennial crop and the yield is largely unaffected by climatic change [65]. It is reported that productivity of oil palm plantation to produce vegetables oils is far higher than other oil bearing crops. For example, productivity of palm oil is reported at about 4.09 ton/ ha, while soy bean produce vegetable oil at about 0.39 ton per ha [66], meaning to produce the same mass production, palm oil plantation need a smaller area compared to other crops. Further, current palm oil plantations have developed sustainable practices to maintain soil and environmental quality, for example by utilising the biomass waste for fertilizer [65,66]. It is believed that palm oil cultivation can maintain soil nutrients, reduce soil erosion and enhance the soil structure, while other the cultivation of seasonal oilseeds can degrade soil

conditions after harvesting [65]. Finally, it is reported that the cultivation of palm oil can reduce greenhouse gas emission by around 2.3 x 10^6 tonnes in 2000, and is known as a net-sequester of carbon dioxide [67] Nevertheless the challenges still remains as a large amount of solid waste biomass is produced every year from palm oil plantation including in form of oil palm empty fruit bunches (EFB). EFB is one of the most abundant solid biomass waste: approximately 43.24 million tons/year of EFB is generated in Indonesia only. There is growing interest to address the environmental challenges related to massive amount of EFB, converting those into new advanced materials. Furthermore, due to their chemical composition and high content of cellulose (40% - 43%), EFB are ideal biomass resource to produce NCs for various applications[68,69]. Our previous results demonstrated that rod-like low aspect ratio NCs can be successfully derived from EFB, 13 with 10.7 ± 1.8 nm in width and 128.4 ± 17.2 nm in length. It should be however noted that cellulose extraction can be performed by different agriculture waste, so the approach here proposed can be extended to several crops. [70]

In this work, mCMC inks were reinforced both to with neat NCs and with NCs functionalized with methacrylic moieties, to create chemical bonding between matrix and fillers. This will also affect printability and rheological, swelling and mechanical properties of the synthesized materials, as evidenced in this study. To the best of our knowledge, this is the first attempt to develop an entirely cellulose-derived nanocomposite ink for DLP 3D printing.

Materials and methods

Materials

Medium viscosity CMC sodium salt powder, low viscosity, trimethoxysilylpropyl methacrylate (98%, molecular weight M_w = 248.35), methacrylic anhydride (M_w= 154.16) and Brilliant Green dye were purchased from Sigma Aldrich (St.Louis, MO, USA). Bismesitoylphosphinic acid (BAPO-OH) photoinitiator [71] was synthesized in Prof. Gruetzmacher's group (ETH Zurich) and kindly provided.

Cellulose Nanocrystals production

The NCs were prepared based on our previously published protocols[68,72]. It consists of two subsequent processes: the isolation of cellulose extracted from EFB, followed by deconstruction of cellulose into cellulose nanocrystal via acid hydrolysis. The extraction of cellulose from EFB was conducted by pre-treatment via alkaline process with 10% wt. NaOH at 150 °C and a pressure of 4 bar for 30 min, followed by bleaching process using H_2O_2 for 2 hours at 80 °C. After that, the isolated cellulose derived from EFB was hydrolyzed using H_2SO_4 36% with a solid/liquid ratio of 1:80 at 50 °C for 3.5 hours. The obtained NCs were then neutralized by simultaneous centrifugation and dialysis. Freeze-drier was then conducted to obtain dried NCs.

Methacrylation protocol

The NCs' methacrylation was based on the protocol by Chang An Xu *et al*.[73] NCs were methacrylated by adding 0.5 g of trimethoxysilylpropyl methacrylate in 50 ml of 2 wt% aqueous solution of pristine NC. The pH was adjusted to 3.0 and the reaction proceeded for 24 hours under magnetic stirring, at room temperature. Finally, the solution was dialyzed against water for 5 days.

CMC was modified as described elsewhere [20]. Briefly, CMC was solubilized in 200 ml of distilled water to obtain a 2wt% solution. Afterwards, 8 ml of methacrylic anhydride were added at 0 °C; the reaction was then carried on for 24 hours at 4°C (pH= 8.0). At last, modified CMC were washed with ethanol, dialyzed for 7 days and freeze-dryed for 5 days.

Hydrogels preparation

Three water-solutions of methacrylated carboxymethyl cellulose, (methacrylated or pristine) cellulose nanocrystals and BAPO-OH were prepared to obtain the corresponding hydrogels, according to the compositions reported in Table 1.

The mixtures were left under magnetic stirring at 40 °C to obtain homogenous solutions.

Table 1. Hydrogels' formulations

Type	mCMC (wt%)	NC (wt%)	mNC (wt%)	Water (wt%)	BAPO-OH (phr*)
Control hydrogels	2	/	/	98	2
NC hydrogels	2	1	/	97	2
mNC hydrogels	2	/	1	97	2

*parts per hundred resins respect to m-CMC

DLP 3D printing

An ASIGA MAX^{TM} 3D-printer (Asiga, Alexandria, AUS), with a light source of 385 nm and xy resolution of 27 µm, was used to print the hydrogels formulations. Various CAD files were converted in stl. format and sent to the printer.

The light intensity and the slice thickness were respectively settled as 30 mW/cm^2 and 50 µm; the exposure time was selected depending on the hydrogel's composition. After 3D printing, samples were carefully washed by immersing in water for 1 minute in order to eliminate excess of inks and then postcured for 3 minutes under UV light (light intensity 50 mW/cm^2).

Characterization

The morphology of the NCs was observed by means of a transmission electron microscopy (TEM, Jeol Jem 1010, JEOL, Tokyo, JPN), operated at an accelerating voltage of 80 kV. The NCs suspension was deposited on a 400-mesh gold glider grid and then stained with 2% aqueous uranyl acetate.

Fourier Transform Infrared (FT-IR) spectra were collected in order to identify the characteristic groups related to the methacrylic functionalization. The spectra were recorded using a Thermo Scientific Nicolet iS50 FTIR Spectrometer (Thermo Fisher Scientific, Waltham, MA, USA) equipped with a diamond crystal ATR (Attenuated Total Reflectance) accessory, with resolution of 4 cm^{-1} and in the range of 4000–500 cm^{-1}.

NCs and mNCs samples were analyzed by Bruker Advance 400 Fourier Transform NMR spectrometer (FT NMR, Bruker, Billerica, MA, USA) operating at 400 MHz. The ^{1}H-NMR was conducted at room temperature. About 1 mg of each sample was dissolved in 1 mL of Dimethyl sulfoxide-d_6 (DMSO-d_6).

Rheological measurements were performed to assess the viscoelastic properties of the materials. Shear, time, amplitude and frequency sweep tests were performed through a rheometer (Physica MCR 302, Anton Paar, Graz, AUT) in parallel plate mode. For the experiments, the gap between the plates was fixed at 0.3 mm. For the photorheological tests, the instrument was equipped with a quartz bottom plate, on which the formulation was placed. A UV-light source (Hamamatsu LC8 lamp, Hamamatsu Photonics, Shizuoka, JPN) at

light intensity of 30 mWcm^{-2} was placed under the quartz plate and switched on after 60 s to allow the system to stabilize before the onset of polymerization. Time sweep measurements were performed during irradiation at a constant frequency of 1 Hz. According to preliminary amplitude sweep tests, the experiments were performed within the linear viscoelastic region (strain amplitude γ of 1%).

The cured hydrogels were, thereafter, subjected to amplitude sweep (frequency ω = 1 Hz) and frequency sweep (frequency ω= 0.01-10 Hz) tests. The Young Modulus E and the crosslinking density ν_e were evaluated from the latter test, following the equations[74],[75]:

$$E = 2\,G'_p(1+v) \tag{1}$$

$$\nu_e = \frac{G'_p\,N_A}{RT} \tag{2}$$

where G'_p is the plateau-value of the storage modulus recorded in frequency sweep tests and the Poisson ratio v is considered equal to 0.5, because hydrogels can be regarded similar to uncompressible, rubber-like material[74].

After the 3D printing, the swelling degree of the hydrogels was evaluated in distilled water, at room temperature. 3D printed hydrated cylindrical hydrogels were immersed in water and, after regular time, they were removed, dried with filter paper and weighted, until the swollen samples reached a constant weight. The degree of swelling (SD) was calculated as follows:

$$SD = \frac{W_t - W_0}{W_0} * 100 \tag{3}$$

Where W_t is the swollen hydrogel's weight at time t and W_0 is the initial weight.
Further, the swelling kinetics of the hydrogels was analyzed by means of Korsmeyer–Peppas and Schott's second order dynamic models.
The pH-sensitivity was investigated by soaking the printed hydrogels in solutions of various pH (1,4,7,11) for 3 hours and then dried and weighed. The SD was measured equally to the swelling experiments.
Compression stress-strain curves were performed employing the rheometer (Physica MCR 302, Anton Paar, Graz, AUT) in compression mode. Each hydrogel was tested in two different hydration conditions: just printed and at the equilibrium weight after swelling in water.
Specimens were 3D-printed in cylinders (8 x 3.5 mm d x h). The stress and the strain at the samples' failure were derived from the normal force [N] and the plates' gap [mm] (corresponding to the height of the samples), that were collected during the experiments, and from the geometrical features of the uncompressed specimens.
The maximum load and the test speed were set to 5 N and 0.1 mm/min, respectively. During the measurements, plates were covered with sandpaper to prevent slipping during the tests.

An ultra-high-resolution Field Emission Scanning Electron Microscope (FESEM, Zeiss Supra 40, Carl Zeiss AG, Oberkochen, DEU) was utilized to observe the morphology of the hydrogels. In order to acquire the SEM

images, the 3D-printed samples were freeze-dried by means of a freeze dryer (Coolsafe 55-4 Pro, LaboGene, Lillerød, DNK), at -50 °C, and then coated with a Pt/Pd coating at a thickness of 5 nm.

Results

The morphology of the extracted EFB- NCs was evaluated by TEM analysis that showed their needle-like shape with average length of ~300nm (Supplementary Figure S1). Part of the extracted NCs underwent the methacrylation process in order to produce fillers which can chemically be bonded to the CMC matrix. To investigate this surface functionalization, FT-IR and NMR analyses were performed.

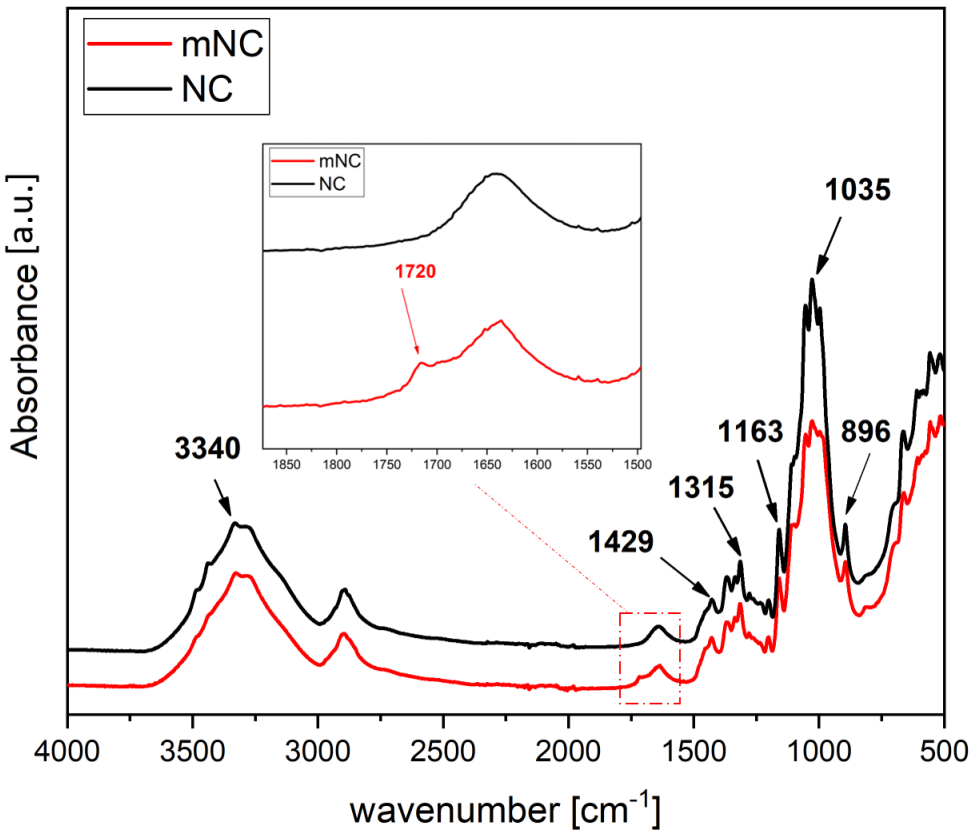

Figure 1. FTIR spectra of pristine cellulose nanocrystals (NCs, black) and functionalized cellulose nanocrystals (m-NCs, red)

NCs and mNCs were both analyzed after dialysis step. As expected, the characteristic peaks of cellulose (at 3340 cm^{-1}, 1429 cm^{-1}, 1315 cm^{-1}, 1035 cm^{-1} and 896 cm^{-1}) and of the SO_2 group (1163 cm^{-1}) are present in both spectra (Fig. 1)[76]. A more detailed description of the two spectra is reported in the Supplementary Information. After chemical modification, a peak at 1720 cm^{-1} appears, associated with the –(C=O)O ester group of methacrylic moieties [20], as evidenced in the magnification of the spectra. This indicates the effective of functionalization step between trimethoxysilylpropyl methacrylate and hydroxyl groups of cellulose. This result was confirmed by ^{1}H-NMR (Supplementary Figure S2).

Having demonstrated the effectiveness of the functionalization, both the pristine and methacrylated cellulose nanocrystals were added to methacrylated CMC as reinforcing phase in photocurable hydrogels.

Figure 2 illustrates the composition of the three hydrogels, in terms of matrix and fillers; the sketches represent the networks that are expected with the three formulations. Based on preliminary tests, the amount of the reinforcers was fixed at 1wt% to not increase excessively the viscosity of the formulations (Supplementary Figure S3), which can be negative for the printing step[77].

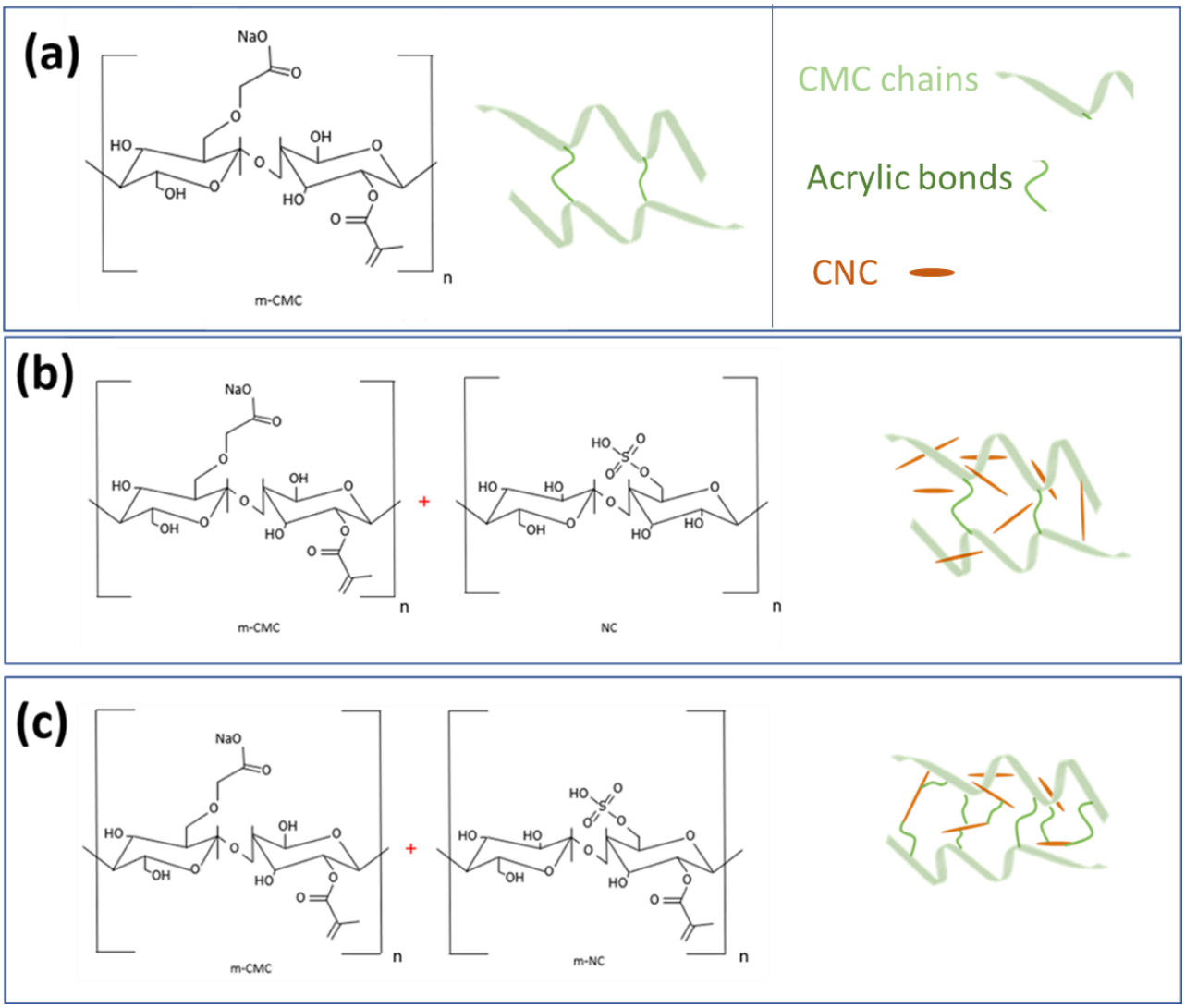

Figure 2. Schematic composition of (a) m-CMC (Control), (b) NC/m-CMC (NC) and (c) m-NC/m-CMC (mNC) hydrogels. The solvent (distilled water) and the photoinitiator (bismesitoylphosphinic acid BAPO-OH) were omitted for the sake of simplicity.

The produced formulations were characterized performing (photo-)rheological analyses, that provided useful information for 3D printing, related to reaction's kinetics and rheological properties of the photo-cured gel. As assessed by the results of real-time sweep tests (Figure 3a), all the formulations form a gel upon UV irradiation in relatively short times, resulting in principle suitable for DLP 3D printing. The presence of the fillers induces slight variations in the photo-curing kinetics of the methacrylated CMC matrix while affecting the final mechanical properties of the cured hydrogels, which can be represented evaluating the plateau value of G' (G'_p). In the case of NC hydrogels, a slight delay of the gel point (time at which G' is equal to G'') (Figure 3b) and a decrease of slope of the G' curve can be detected. On the contrary, considering the m-NC formulations, the photopolymerization occurs faster than in the neat hydrogels. This can be explained considering the presence of methacrylic reactive moieties on NCs' surface, which lead to faster gelation, with the formation of a crosslinked network between mCMC and NCs. As for the rheological properties, both

reinforcers enhance the value of G'_p, which can be considered rough indication of the stiffness of the cured hydrogels. This result was confirmed by the amplitude and frequency sweep tests (Figure 3c, 3d), which both showed better mechanical properties of the hydrogel reinforced with mNCs. In those measurements, the higher values of G' in reinforced hydrogels compared to the neat CMC hydrogel can be related to the presence of the reinforcing fillers, but also to an increase of intramolecular hydrogen bonds with the cellulose nanocrystals[60]. The presence of additional covalent bonds in the m-NC hydrogels can be demonstrated by the highest crosslinking density ν_e of mNC hydrogels (Table 2) measured in frequency sweeps tests (see method section). For the three hydrogels G' remains stable across a large range of deformation (Fig. 3c), indicating that a stable gel has formed after the UV exposure. The nano-reinforced specimens can withstand lower strain amplitude before the yielding (highlighted by the G' dropdown). In particular, the mNC hydrogels present a sharper G' downturn, indicating that the higher rigidity lead to a more brittle behavior. The frequency sweeps attested that the three hydrogels behave as strong, viscoelastic solids for a wide range of frequencies, with G' being stable and larger than G'' up to 10 Hz (Fig. 3d). The storage modulus values recorded in this test provide a first measurement of the Young modulus, which, for the mNC hydrogels, resulted to be about 3-fold times larger than that of the unfilled samples (Table 2).

Finally, the viscoelastic behavior of the hydrogels was defined by evaluating the loss factor:

$$tan\,\delta = \frac{G''}{G'} \quad (4)$$

For ideally viscous material, δ=90°, while δ=0° corresponds to an ideally elastic one. For the three hydrogels δ is lower than 5°, indicating a strongly elastic and solid behavior.

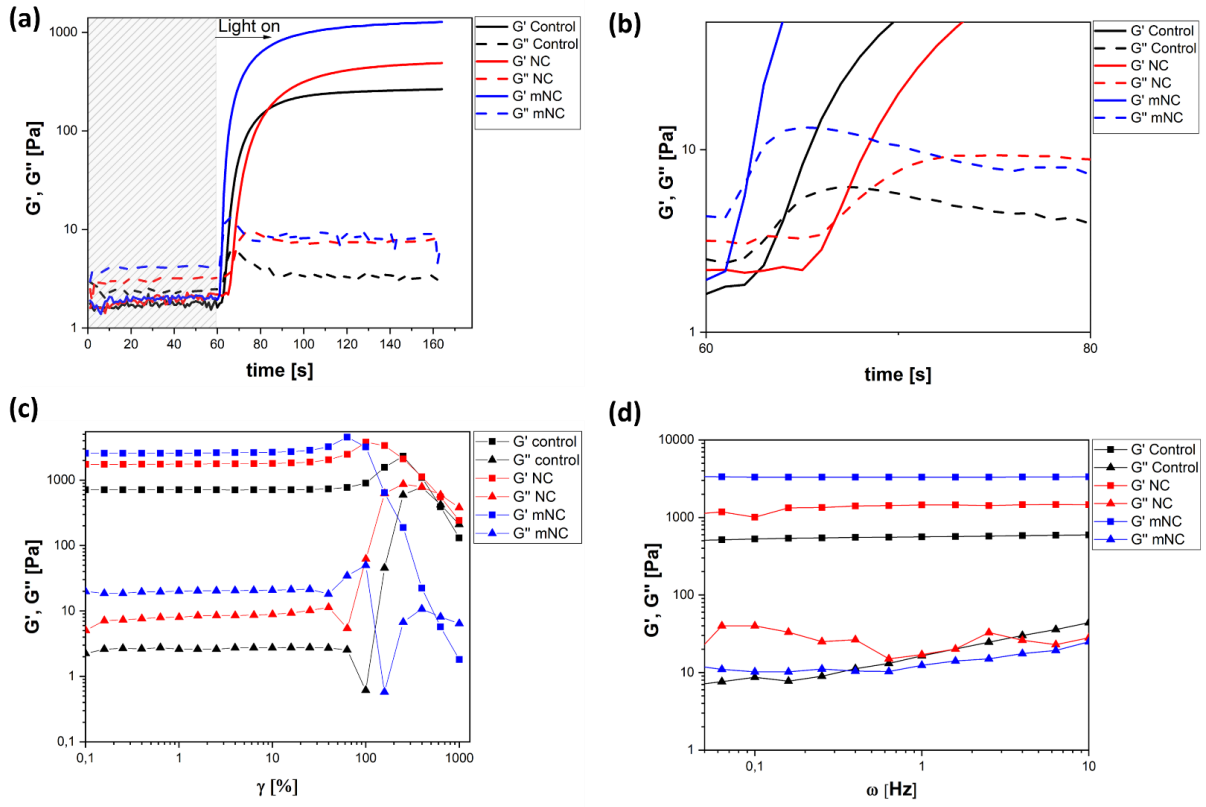

Figure 3. (a) Real-time photorheology of m-CMC (Control), NC/m-CMC (NC) and m-NC/m-CMC (mNC) hydrogels, (b) their gel points (G'=G'') during the UV irradiation, (c) amplitude sweeps test (frequency 1 Hz, strain amplitude 0.1-1000%) and (d) frequency sweep tests (strain amplitude 1%, frequency 0.01-10 Hz) of the cured hydrogels.

Table 2. Crosslinking density and Young Modulus of the cellulose-based hydrogels

Hydrogel	ν_e [μ^{-3}]	E [KPa]
Control	1.70 ± 0.6	2.36 ± 0.82
NC	3.13 ± 0.04	4.34 ± 0.06
mNC	5.72 ± 1.01	7.78 ± 2.05

Having confirmed the good reactivity and stability of the nanocomposite hydrogels, the formulations were successfully 3D printed through DLP. The exposure time was adjusted depending on the composition of the hydrogel aiming to obtain self-supporting structures in short times. The exposure time for each layer was then empirically fixed at 12 seconds (light intensity of 30 mW/cm^2) for mNC hydrogels, whereas, according to photorheology measurements, Control and NC formulations required longer expositions to the light (13 and 15 seconds, respectively). As shown in figure 4a-c, the mNC formulation was shaped in both simple cylindric structures and more complex geometries. The digital models are reported in figure S6. When compared to the neat counterparts (Supplementary Figure S5), the 3D printed composites appear opaque and, thanks to the better mechanical properties, allow an easier handling of the structures, especially in the detachment of the objects from build platform.

Furthermore, the addition of modified reinforcers shortened the printing times, as expected after photorheology results, enabling the fabrication of more complex geometries. Since the methacrylated fillers co-polymerize with the m-CMC matrix, those can act both as reinforcing fillers, and as crosslinkers, inducing a more dense network which is helpful for obtaining better resolution [77]. Despite the high amount of water, the presence of the mNCs and the accurate control of the printing parameters enabled the fabrication of self-standing objects and parts with relatively sharp angles and thin walls. Nevertheless, the shape fidelity of these formulations was poor, mainly due to uncontrolled polymerization. To prevent this issue, a water-soluble dye (brilliant green BG) was added to the mNC formulations to properly confine the polymerization.[78] BG is a cationic dye, commonly used in textile and paper industries, [79] already applied in DLP-3D printing. [77,80] The presence of BG enabled the fabrication of more complex objects with a good resolution, also in z-direction. This results in neater contours, with the printing of both squared and rounded shapes in the same part (Figure 4d,e). Moreover, BG didn't affect the photopolymerization process, as shown in Figure S4, ensuring a good trade-off between the resolution and the fabrication speed.

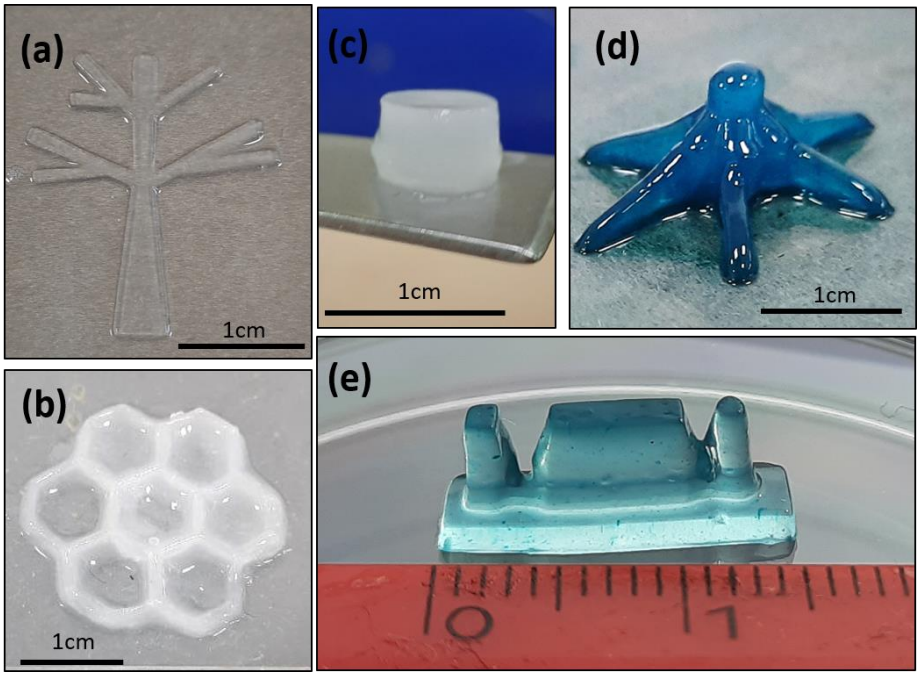

Figure 4. (a-c) 3D-printed m-NC (1wt%)/m-CMC (2wt%) hydrogels (d-e) 3D-printed mNC hydrogels containing a brilliant green dye

Swelling ability of the 3D printed components was then tested. This property is crucial because most of the hydrogels' applications rely on their ability to absorb/hold large amounts of fluids [36]. As it can be observed from the experimental data (Figure 5a), the swelling degree reaches the equilibrium value after 3 hours and then remains stable for days, indicating that all the hydrogels can absorb a large amount of water without being destroyed. On the other hand, the swelling degree decreases significantly with the presence of nanofillers, decreasing from the 450% of the neat hydrogels to the 300% and to the 150% of the NC and mNC specimens, respectively. This reduction was expected and can be related to the higher crosslinking density of the nanocomposites, which limits network expansion and, thus, the water absorption[50]. Moreover, in the composite hydrogels the water penetration is hampered due to the reduction of the free space between the m-CMC chains, occupied by the nanofillers[76]. At last, it should be also considered that mNC specimens are less hydrophilic due to partial substitution of hydroxyl groups with methacrylic moieties. Each of these aspects, namely the abundance of hydrophilic groups, the crosslinking density and the rigidity of the network are known to have an impact on the swelling degree of hydrogels, decreasing their performance[81]. So,

according to possible applications, a suitable trade-off must be performed considering swellability, mechanical properties and printability of the presented hydrogels.

Most of the applications of hydrogels rely on their ability to hold water and/or to vary their volume once they absorb and release a solvent (e.g. delivery of drugs)[81]. Therefore, it is important to model the swelling behavior and kinetics of the hydrogels according to predictable, mathematical models. Depending the investigations on the 3D printed specimens, the swelling kinetics was evaluated by means of two well-known kinetic models: the Peppas-Korsmeyer and the Schott's models (equation S1 and S2, respectively). The curves (Figs. 5b,c) of the two models were obtained from the experimental data and used to extrapolate the coefficient of determination (R^2) and the constants of the two equations, reported in Table 3. Literature shows that for other cellulose-based hydrogels [82,83], for the control and NC hydrogels, n is lower than 0.5, revealing a fickian diffusion mechanism. For mNC sample, n=0.54, indicating that the water diffusion into these hydrogels follows a non-fickian diffusion type. The larger value of n could be ascribed to the higher rigidity and crosslinking density of the network, that withstanding the chains' relaxation within the hydrogel. The time-dependence of the phenomenon can also be described through Schott's model. According to the equation S2, the swelling degree decreases over time according to a second-order equation. The high R^2 values of the linear regressions indicate that more than the 99% of the experimental data can be explained by the model, assessing its reliability. Finally, the swelling rate constants k_1 and k_2 are a function of several aspects, such as hydrophilicity, degree of crosslinking and gel's flexibility. As it can be deduced from the models' equations, larger and smaller values of k_1 and k_2 correspond to a faster and easier water penetration. The calculations show a trend that is consistent with the previous swelling experiments, confirming that the cellulose nanocrystals, especially the modified ones, slow down the swelling process.

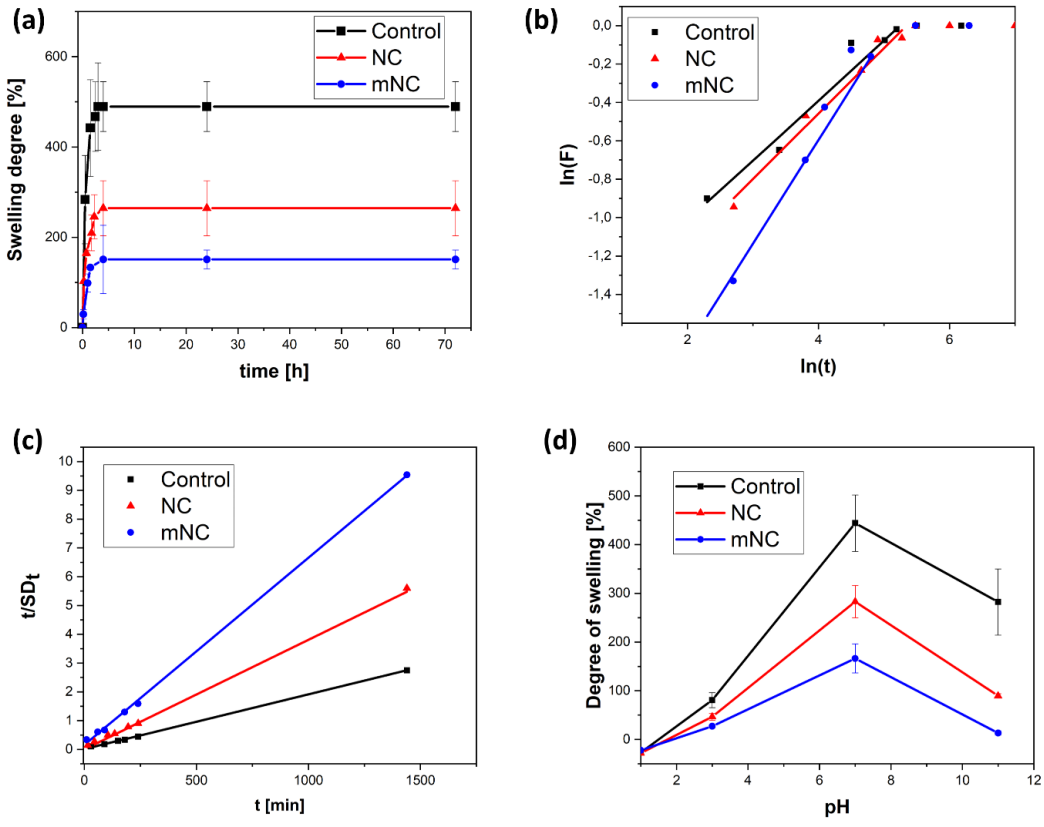

Figure 5. (a) swelling in distilled water of the 3D-printed hydrogels as printed (b) Peppas-Korsmeyer plot of (b) ln(F) against ln(t); (c) Schott's model plot of $t/(SD)_t$ against t (d) relation between the equilibrium degree of swelling and the pH for m-CMC (Control), NC/m-CMC (NC) and m-NC/m-CMC (mNC) hydrogels.

Table 3. kinetics parameters for the swelling of the cellulose-based hydrogels in distilled water

	Korsmeyer-Peppas model			Schott's model	
	R^2	N	K_1	R^2	$K_2 \times 10^4$
Control	0.899	0.31	0.2	0.999	9.47
NC	0.978	0.34	0.17	0.999	2.77
m-NC	0.935	0.54	0.06	0.999	1.87

Another important characteristic of cellulose-based hydrogels is the pH-sensitivity, i.e. the ability to give volume or swelling variations at different pHs. This feature was exploited in many applications, such as sensors and controlled drug-release devices[29,83]. This property is related to the fact that carboxymethyl cellulose is an anionic polymer that, at pH>4.6 (equivalent to the pKa of the carboxylic acid), possesses fixed negative charges $-COO^-$, derived from the ionization of the carboxyl groups -COOH. When the pH is above 4.6, the electrostatic repulsion between the negatively charged sites promotes the swelling; instead, at lower pH, the protonation of most of the COO^- ions reduces the electrostatic repulsion, thus inhibiting the swelling ratio[84]. All the synthesized 3D printed hydrogels keep the properties of CMC, demonstrating to be pH-sensitive. As displayed in figure 5d, the water absorption of the hydrogels increases with pH, until a maximum value at pH 7.0. When the hydrogels are immersed in alkaline solutions, the swelling degree decreases slightly, due to the combination between the positive-charged metal ions of the solutions and the COO^- groups of the CMC. This, again, limits the repulsion between the negative groups and the hydrogels' expansion[84]. Even the nanoreinforcers, that are extracted by acid hydrolysis, possess sulfate negative groups that were demonstrated to be less sensitive to pH variations (pKa=1.9)[85]. Their presence does not play an evident role in the pH-responsiveness of the tested parts, since all the specimens follow a similar trend, even if with different values related to the different mechanical properties.

The SEM images of lyophilized 3D-printed specimens showed the typical microporous morphology of the hydrogels, that is responsible for the large solvent absorption. Fig. 6 shows that the morphology of the lyophilized 3D-printed specimens contains macroscopic networks that are highly anisotropic and rough possibly due to the shock removal of excessive water content upon freeze drying. Similar characteristics for alginate hydrogels were reported by Sergeeva et.al[86]. Compared to the control system (Fig. 6a), the inclusion of NCs into the systems (Fig. 6b) created the extended fibrillar network, due to the presence of numerous intertwined fibers. This can be related to the presence of inter-molecular hydrogen bond interaction among the NCs, which create aggregates once lyophilized. Instead, the sample with mNC (Figure 6c) shows a morphology similar to the control. In this case, it must be considered that the fillers reacted with the mCMC, as witnessed by increase of cross-linking density, forming a hybrid network between fillers and matrix. This inhibits aggregation of fillers, resulting in a more homogenous and smooth morphology.

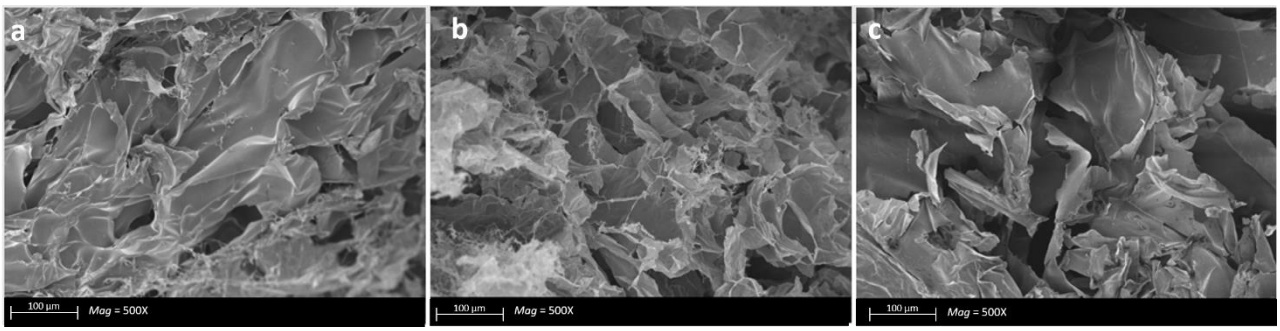

Figure 6. FE-SEM pictures of (a) Control, (b) NC and (c) mNC 3D printed hydrogels.

Finally, the mechanical properties of the nanocomposites were assessed by measuring compressive strength and deformation of the hydrogels, 3D printed in the form of cylinders specimens. The typical stress-strain curves are reported in Fig. 7a. Equally to the control hydrogels, the composite specimens show a relevant deformation rate (strain at failure ε_f > 50%), and a unilinear elastic region. The bare NCs improved the mechanical performances of the hydrogels, especially the compressive strength (figure 7b), that is up to 65 kPa, about 1.5 folds the resistance of the control samples. As discussed above, this is related both to the presence of a phase with improved mechanical properties and to its interactions with the matrix. In fact, the cellulose nanocrystals possess hydroxylic groups that tend to form hydrogen bonds with the hydroxylic and carboxylic groups of the m-CMC, enabling the efficient transfer of the compressive load. As for the mNC hydrogels, it can be observed the highest resistance to deformation (figure 7c), linked to the highest rigidity of the material. The properties of the specimens in study are in line with those of other natural hydrogels containing similar amount of water. [19,60,87] The mechanical properties were also evaluated in swollen conditions at the equilibrium, as reported in Figure 7d,e,f. Here it must be recall that the different hydrogels absorb different amounts of water (Fig. 5a), so their mechanical performance cannot be directly compared since it is well known that the increase of water content in a hydrogel leads to a decrease of mechanical properties [88]. Nevertheless, it is worthy to measure the mechanical properties of the completely swelled specimens and take some consideration. As expected, at the equilibrium state all the specimens showed a decrease of ultimate stress (Fig. 7e), but the mNC specimens still show better mechanical performance, with a decrease of ultimate stress of only 30% compared to the just printed counterpart. Furthermore, differently from the other hydrogels, the specimens with mNCs maintains also a good ultimate strain (fig. 7f). This indicates that this hydrogel, in which a co-continuous network is formed between fillers and mCMC matrix, is particularly promising since it can preserve good mechanical properties also in swollen condition, showing at the same time the best printability.

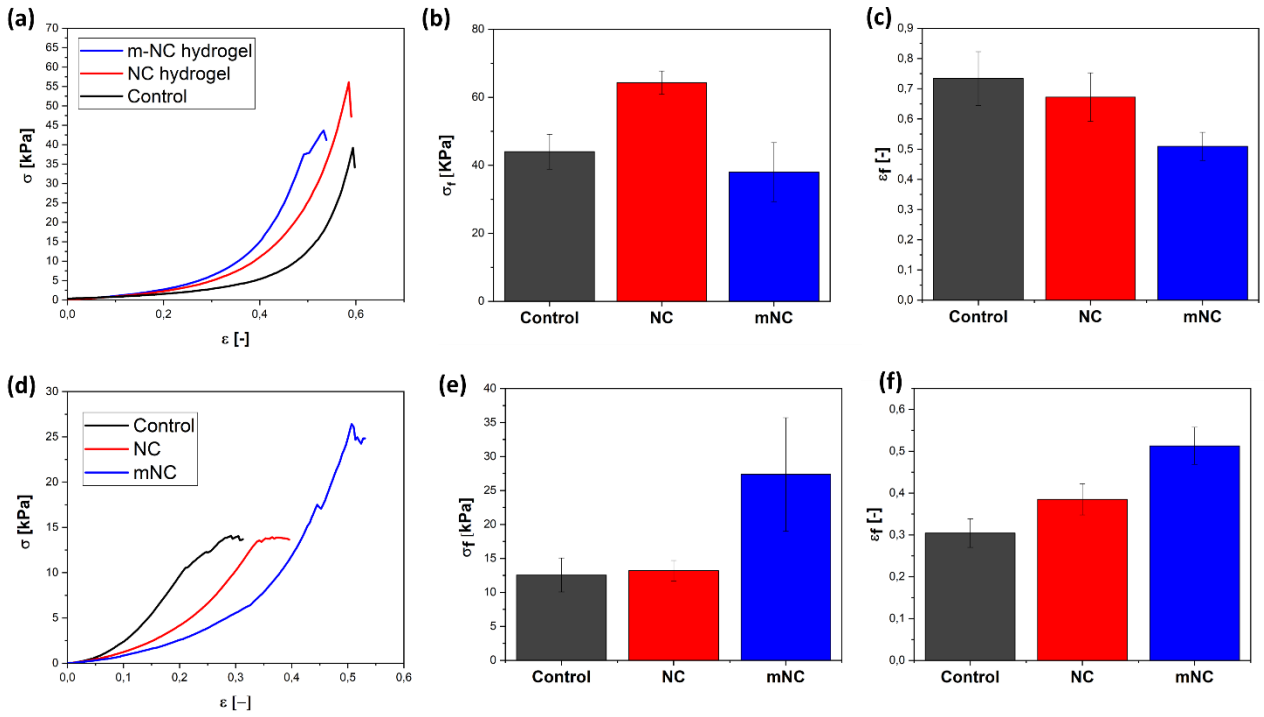

Figure 7. (a) plot of stress σ versus strain ε of the hydrogels as printed (b)ultimate stress σ_f of the hydrogels as printed (c)strain at failure ε_f of the hydrogels as printed (d) plot of stress versus strain of the printed hydrogels after swelling (e) ultimate stress of the printed hydrogels after swelling (f) ultimate strain of the printed hydrogels after swelling.

Conclusions

3D printing is forecasted to have a huge impact on industries, with a market projected to grow to 5.2 billion US within the 2026 [89]. Due to its expanding applications, it is fundamental considering the eco-sustainability of 3D printing, which, actually, has been largely analyzed [90–92], identifying a 70% of decrease of the environmental impact in comparison to conventional processes [90]. However the market is still largely based on materials from fossil resources, especially in vat photopolymerization 3D Printing. The growing interest towards cellulose, whose market size was estimated 5.7 billion in 2021 [93,94], is particularly appealing in this context, with the opportunity to develop novel fully biobased materials. Here it was presented the successful synthesis of new all-cellulose waterborne nanocomposites inks for DLP 3D printing. These materials are based on methacrylated carboxy methyl cellulose reinforced with cellulose nanocrystals, extracted from biowaste, which were used both pristine and after surface methacrylation. Those ingredients were used to produce photocurable formulation, which properties were preliminary studied by photorhelogy evidencing a small delay of light induced polymerization in the presence of the cellulose reinforces. Nevertheless all the developed inks results suitable for light activated 3D printing. Both the nanocomposite hydrogels, were 3D-printed through DLP, showing the necessity of the presence of dye to improve the resolution of the structures. Compared to the neat hydrogels, both the nanocomposites showed improved mechanical properties, while the water uptake is reduced by the addition of the NCs. Furthermore, all the inks show pH sensitivity. It was observed that the methacrylated fillers enhance the reactivity to the UV radiation and lead to the highest rigidity and crosslinking density, but induced a decrease of the swelling degree. The specimens with pristine cellulose nanocrystals instead grant higher degree of swelling and compression strength.

To the best of our knowledge, this is the first study which reports full cellulose-based nanocomposite inks for vat 3D printing, opening the way to the development of more sustainable inks in an industry that is still almost completely based on synthetic polymers. Furthermore, according to the envisaged applications, it was demonstrated that the property of the 3D printed structures can be conveniently tuned, enlarging the possible use of such formulations. In this work cellulose NCs were extracted by EFB waste, but the same approach can be applied to several alternative agriculture wastes. Owing to the ease of supply, low price and sustainable characteristics, cellulose and its derivatives and nano-forms show immense growth potential and, combined with 3D printing, they can provide innovative pathways to an eco-sustainable approach for on-demand manufacturing in a varied range of sectors, such as electronics, tissue engineering and pharmaceutics [94]

Acknowledgments

This research was developed in the frame of "Fernandes Fellowship" funding Scheme of Institute of Advanced Studies, University of Warwick. Athanasia Amanda Septevani is grateful for the funds to visit Politecnico di Torino, Italy from the scheme of "LIPI Global Collaboration 2019" as well as "Program Non-Gelar Research and Innovation in Science and Technology Project BRIN 2021".

References

[1] Y.Z. Yu, J.R. Lu, J. Liu, 3D printing for functional electronics by injection and package of liquid metals into channels of mechanical structures, Mater. Des. 122 (2017) 80–89. https://doi.org/10.1016/j.matdes.2017.03.005.

[2] D.J. Roach, C. Roberts, J. Wong, X. Kuang, J. Kovitz, Q. Zhang, T.G. Spence, H.J. Qi, Surface modification of fused filament fabrication (FFF) 3D printed substrates by inkjet printing polyimide for printed electronics, Addit. Manuf. 36 (2020) 101544. https://doi.org/10.1016/j.addma.2020.101544.

[3] E.O. Bachtiar, O. Erol, M. Millrod, R. Tao, D.H. Gracias, L.H. Romer, S.H. Kang, 3D printing and characterization of a soft and biostable elastomer with high flexibility and strength for biomedical applications, J. Mech. Behav. Biomed. Mater. 104 (2020) 103649. https://doi.org/10.1016/j.jmbbm.2020.103649.

[4] S. Singh, C. Prakash, S. Ramakrishna, 3D printing of polyether-ether-ketone for biomedical applications, Eur. Polym. J. 114 (2019) 234–248. https://doi.org/10.1016/j.eurpolymj.2019.02.035.

[5] Z. Hou, X. Tian, J. Zhang, Z. Zheng, L. Zhe, D. Li, A. V. Malakhov, A.N. Polilov, Optimization design and 3D printing of curvilinear fiber reinforced variable stiffness composites, Compos.

Sci. Technol. 201 (2021) 108502. https://doi.org/10.1016/j.compscitech.2020.108502.

[6] J.J. Nijdam, D. Agarwal, B.S. Schon, Assessment of a novel window of dimensional stability for screening food inks for 3D printing, J. Food Eng. 292 (2021) 110349. https://doi.org/10.1016/j.jfoodeng.2020.110349.

[7] P. Rando, M. Ramaioli, Food 3D printing: Effect of heat transfer on print stability of chocolate, J. Food Eng. 294 (2021) 110415. https://doi.org/10.1016/j.jfoodeng.2020.110415.

[8] S. Kim, H. Seong, Y. Her, J. Chun, A study of the development and improvement of fashion products using a FDM type 3D printer, Fash. Text. 6 (2019). https://doi.org/10.1186/s40691-018-0162-0.

[9] V.S.D. Voet, J. Guit, K. Loos, Sustainable Photopolymers in 3D Printing: A Review on Biobased, Biodegradable, and Recyclable Alternatives, Macromol. Rapid Commun. 42 (2021) 1–11. https://doi.org/10.1002/marc.202000475.

[10] S. Miao, W. Zhu, N.J. Castro, M. Nowicki, X. Zhou, H. Cui, J.P. Fisher, L.G. Zhang, 4D printing smart biomedical scaffolds with novel soybean oil epoxidized acrylate, Sci. Rep. 6 (2016) 1–10. https://doi.org/10.1038/srep27226.

[11] C. Noè, A. Cosola, C. Tonda-Turo, R. Sesana, C. Delprete, A. Chiappone, M. Hakkarainen, M. Sangermano, DLP-printable fully biobased soybean oil composites, Polymer (Guildf). 247 (2022) 124779. https://doi.org/10.1016/j.polymer.2022.124779.

[12] A. Cosola, R. Conti, H. Grützmacher, M. Sangermano, I. Roppolo, C.F. Pirri, A. Chiappone, Multiacrylated Cyclodextrin: A Bio-Derived Photocurable Macromer for VAT 3D Printing, Macromol. Mater. Eng. 305 (2020) 2000350. https://doi.org/https://doi.org/10.1002/mame.202000350.

[13] A. C. Weems, K. R. Delle Chiaie, R. Yee, A. P. Dove, Selective Reactivity of Myrcene for Vat Photopolymerization 3D Printing and Postfabrication Surface Modification, Biomacromolecules. 21 (2019) 163–170. https://doi.org/10.1021/acs.biomac.9b01125.

[14] V. S. D. Voet, T. Strating, G. H. M. Schnelting, P. Dijkstra, M. Tietema, J. Xu, A. J. J. Woortman, K. Loos, J. Jager, R. Folkersma, Biobased Acrylate Photocurable Resin Formulation for Stereolithography 3D Printing, ACS Omega. 3 (2018) 1403–1408.

https://doi.org/10.1021/acsomega.7b01648.

[15] L. Breloy, V. Brezová, Z. Barbieriková, Y. Ito, J. Akimoto, A. Chiappone, S. Abbad-Andaloussi, J.-P. Malval, D.-L. Versace, Methacrylated Quinizarin Derivatives for Visible-Light Mediated Photopolymerization: Promising Applications in 3D-Printing Biosourced Materials under LED@405 nm, ACS Appl. Polym. Mater. 4 (2021) 210–228. https://doi.org/10.1021/acsapm.1c01210.

[16] S.H. Kim, Y.K. Yeon, J.M. Lee, J.R. Chao, Y.J. Lee, Y.B. Seo, M.T. Sultan, O.J. Lee, J.S. Lee, S. Il Yoon, I.S. Hong, G. Khang, S.J. Lee, J.J. Yoo, C.H. Park, Precisely printable and biocompatible silk fibroin bioink for digital light processing 3D printing, Nat. Commun. 9 (2018). https://doi.org/10.1038/s41467-018-03759-y.

[17] S. Krishnamoorthy, S. Wadnap, B. Noorani, H. Xu, C. Xu, Investigation of gelatin methacrylate working curves in dynamic optical projection stereolithography of vascular-like constructs, Eur. Polym. J. 124 (2020) 109487. https://doi.org/10.1016/j.eurpolymj.2020.109487.

[18] R. Gauvin, Y.C. Chen, J.W. Lee, P. Soman, P. Zorlutuna, J.W. Nichol, H. Bae, S. Chen, A. Khademhosseini, Microfabrication of complex porous tissue engineering scaffolds using 3D projection stereolithography, Biomaterials. 33 (2012) 3824–3834. https://doi.org/10.1016/j.biomaterials.2012.01.048.

[19] Y. Shen, H. Tang, X. Huang, R. Hang, X. Zhang, Y. Wang, X. Yao, DLP printing photocurable chitosan to build bio-constructs for tissue engineering, Carbohydr. Polym. 235 (2020) 115970. https://doi.org/10.1016/j.carbpol.2020.115970.

[20] G. Melilli, I. Carmagnola, C. Tonda-Turo, F. Pirri, G. Ciardelli, M. Sangermano, M. Hakkarainen, A. Chiappone, DLP 3D printing meets lignocellulosic biopolymers: Carboxymethyl cellulose inks for 3D biocompatible hydrogels, Polymers (Basel). 12 (2020) 1–11. https://doi.org/10.3390/POLYM12081655.

[21] B. Huang, R. Hu, Z. Xue, J. Zhao, Q. Li, T. Xia, W. Zhang, C. Lu, Continuous liquid interface production of alginate/polyacrylamide hydrogels with supramolecular shape memory properties, Carbohydr. Polym. 231 (2020) 115736. https://doi.org/10.1016/j.carbpol.2019.115736.

[22] X. He, W. Lu, C. Sun, H. Khalesi, A. Mata, R. Andaleeb, Y. Fang, Cellulose and cellulose derivatives: Different colloidal states and food-related applications, Carbohydr. Polym. 255 (2021) 117334. https://doi.org/10.1016/j.carbpol.2020.117334.

[23] W. Xu, X. Wang, N. Sandler, S. Willför, C. Xu, Three-Dimensional Printing of Wood-Derived Biopolymers: A Review Focused on Biomedical Applications, ACS Sustain. Chem. Eng. 6 (2018) 5663–5680. https://doi.org/10.1021/acssuschemeng.7b03924.

[24] C. Gauss, K.L. Pickering, L.P. Muthe, The use of cellulose in bio-derived formulations for 3D/4D printing: A review, Compos. Part C Open Access. 4 (2021) 100113. https://doi.org/10.1016/j.jcomc.2021.100113.

[25] M. Espert, A. Salvador, T. Sanz, Cellulose ether oleogels obtained by emulsion-templated approach without additional thickeners, Food Hydrocoll. 109 (2020) 106085. https://doi.org/10.1016/j.foodhyd.2020.106085.

[26] W. Wang, J. Jung, Y. Zhao, Chitosan-cellulose nanocrystal microencapsulation to improve encapsulation efficiency and stability of entrapped fruit anthocyanins, Carbohydr. Polym. 157 (2017) 1246–1253. https://doi.org/10.1016/j.carbpol.2016.11.005.

[27] E. Małachowska, M. Dubowik, A. Lipkiewicz, K. Przybysz, P. Przybysz, Analysis of cellulose pulp characteristics and processing parameters for efficient paper production, Sustain. 12 (2020) 1–12. https://doi.org/10.3390/su12177219.

[28] H. Paukkonen, A. Ukkonen, G. Szilvay, M. Yliperttula, T. Laaksonen, Hydrophobin-nanofibrillated cellulose stabilized emulsions for encapsulation and release of BCS class II drugs, Eur. J. Pharm. Sci. 100 (2017) 238–248. https://doi.org/10.1016/j.ejps.2017.01.029.

[29] Q. Luan, W. Zhou, H. Zhang, Y. Bao, M. Zheng, J. Shi, H. Tang, F. Huang, Cellulose-Based Composite Macrogels from Cellulose Fiber and Cellulose Nanofiber as Intestine Delivery Vehicles for Probiotics, J. Agric. Food Chem. 66 (2018) 339–345. https://doi.org/10.1021/acs.jafc.7b04754.

[30] A. Zennifer, P. Senthilvelan, S. Sethuraman, D. Sundaramurthi, Key advances of carboxymethyl cellulose in tissue engineering & 3D bioprinting applications, Carbohydr. Polym. 256 (2021) 117561. https://doi.org/10.1016/j.carbpol.2020.117561.

[31] V. Kanikireddy, K. Varaprasad, T. Jayaramudu, C. Karthikeyan, R. Sadiku, Carboxymethyl

cellulose-based materials for infection control and wound healing: A review, Int. J. Biol. Macromol. 164 (2020) 963–975. https://doi.org/10.1016/j.ijbiomac.2020.07.160.

[32] S. Mallakpour, M. Tukhani, C.M. Hussain, Recent advancements in 3D bioprinting technology of carboxymethyl cellulose-based hydrogels: Utilization in tissue engineering, Adv. Colloid Interface Sci. 292 (2021) 102415. https://doi.org/10.1016/j.cis.2021.102415.

[33] H. Samadian, H. Maleki, Z. Allahyari, M. Jaymand, Natural polymers-based light-induced hydrogels: Promising biomaterials for biomedical applications, Coord. Chem. Rev. 420 (2020) 213432. https://doi.org/10.1016/j.ccr.2020.213432.

[34] Z. Shi, X. Gao, M.W. Ullah, S. Li, Q. Wang, G. Yang, Electroconductive natural polymer-based hydrogels, Biomaterials. 111 (2016) 40–54. https://doi.org/10.1016/j.biomaterials.2016.09.020.

[35] G. Janarthanan, H.N. Tran, E. Cha, C. Lee, D. Das, I. Noh, 3D printable and injectable lactoferrin-loaded carboxymethyl cellulose-glycol chitosan hydrogels for tissue engineering applications, Mater. Sci. Eng. C. 113 (2020) 111008. https://doi.org/10.1016/j.msec.2020.111008.

[36] M. Bahram, N. Mohseni, M. Moghtader, An Introduction to Hydrogels and Some Recent Applications, Emerg. Concepts Anal. Appl. Hydrogels. (2016). https://doi.org/10.5772/64301.

[37] R. Curvello, V.S. Raghuwanshi, G. Garnier, Engineering nanocellulose hydrogels for biomedical applications, Adv. Colloid Interface Sci. 267 (2019) 47–61. https://doi.org/10.1016/j.cis.2019.03.002.

[38] M.N. Collins, M. Nechifor, F. Tanasă, M. Zănoagă, A. McLoughlin, M.A. Stróżyk, M. Culebras, C.A. Teacă, Valorization of lignin in polymer and composite systems for advanced engineering applications – A review, Int. J. Biol. Macromol. 131 (2019) 828–849. https://doi.org/10.1016/j.ijbiomac.2019.03.069.

[39] A.C. Hernández-González, L. Téllez-Jurado, L.M. Rodríguez-Lorenzo, Alginate hydrogels for bone tissue engineering, from injectables to bioprinting: A review, Carbohydr. Polym. 229 (2020) 115514. https://doi.org/10.1016/j.carbpol.2019.115514.

[40] A. Serafin, C. Murphy, M.C. Rubio, M.N. Collins, Printable alginate/gelatin hydrogel

reinforced with carbon nanofibers as electrically conductive scaffolds for tissue engineering, Mater. Sci. Eng. C. 122 (2021) 111927. https://doi.org/10.1016/j.msec.2021.111927.

[41] M. Izadifar, D. Chapman, P. Babyn, X. Chen, M.E. Kelly, UV-Assisted 3D Bioprinting of Nanoreinforced Hybrid Cardiac Patch for Myocardial Tissue Engineering, Tissue Eng. - Part C Methods. 24 (2018) 74–88. https://doi.org/10.1089/ten.tec.2017.0346.

[42] S. Asif, P. Chansoria, R. Shirwaiker, Ultrasound-assisted vat photopolymerization 3D printing of preferentially organized carbon fiber reinforced polymer composites, J. Manuf. Process. 56 (2020) 1340–1343. https://doi.org/10.1016/j.jmapro.2020.04.029.

[43] M. Shahbazi, H. Jäger, S.J. Ahmadi, M. Lacroix, Electron beam crosslinking of alginate/nanoclay ink to improve functional properties of 3D printed hydrogel for removing heavy metal ions, Carbohydr. Polym. 240 (2020) 116211. https://doi.org/10.1016/j.carbpol.2020.116211.

[44] F. Afghah, M. Altunbek, C. Dikyol, B. Koc, Preparation and characterization of nanoclay-hydrogel composite support-bath for bioprinting of complex structures, Sci. Rep. 10 (2020) 1–13. https://doi.org/10.1038/s41598-020-61606-x.

[45] W. Wu, Study on 3D printing technology and mechanical properties of a nano-enhanced composite hydrogel bio-ink, Micro Nano Lett. 15 (2020) 925–929. https://doi.org/10.1049/mnl.2019.0712.

[46] U.K. Roopavath, R. Soni, U. Mahanta, A.S. Deshpande, S.N. Rath, 3D printable SiO2 nanoparticle ink for patient specific bone regeneration, RSC Adv. 9 (2019) 23832–23842. https://doi.org/10.1039/c9ra03641e.

[47] S.A. Wilson, L.M. Cross, C.W. Peak, A.K. Gaharwar, Shear-Thinning and Thermo-Reversible Nanoengineered Inks for 3D Bioprinting, ACS Appl. Mater. Interfaces. 9 (2017) 43449–43458. https://doi.org/10.1021/acsami.7b13602.

[48] S. Sayyar, E. Murray, B.C. Thompson, J. Chung, D.L. Officer, S. Gambhir, G.M. Spinks, G.G. Wallace, Processable conducting graphene/chitosan hydrogels for tissue engineering, J. Mater. Chem. B. 3 (2015) 481–490. https://doi.org/10.1039/c4tb01636j.

[49] H. Nosrati, R. Sarraf Mamoory, D.Q. Svend Le, C.E. Bünger, Fabrication of gelatin/hydroxyapatite/3D-graphene scaffolds by a hydrogel 3D-printing method, Mater.

Chem. Phys. 239 (2020) 122305. https://doi.org/10.1016/j.matchemphys.2019.122305.

[50] N.B. Palaganas, J.D. Mangadlao, A.C.C. De Leon, J.O. Palaganas, K.D. Pangilinan, Y.J. Lee, R.C. Advincula, 3D printing of photocurable cellulose nanocrystal composite for fabrication of complex architectures via stereolithography, ACS Appl. Mater. Interfaces. 9 (2017) 34314–34324. https://doi.org/10.1021/acsami.7b09223.

[51] Y. Sun, Y. Chu, W. Wu, H. Xiao, Nanocellulose-based lightweight porous materials: A review, Carbohydr. Polym. 255 (2021) 117489. https://doi.org/10.1016/j.carbpol.2020.117489.

[52] J. Leppiniemi, P. Lahtinen, A. Paajanen, R. Mahlberg, S. Metsä-Kortelainen, T. Pinomaa, H. Pajari, I. Vikholm-Lundin, P. Pursula, V.P. Hytönen, 3D-Printable Bioactivated Nanocellulose-Alginate Hydrogels, ACS Appl. Mater. Interfaces. 9 (2017) 21959–21970. https://doi.org/10.1021/acsami.7b02756.

[53] R. Shen, S. Xue, Y. Xu, Q. Liu, Z. Feng, H. Ren, H. Zhai, F. Kong, Research progress and development demand of nanocellulose reinforced polymer composites, Polymers (Basel). 12 (2020) 1–19. https://doi.org/10.3390/POLYM12092113.

[54] T.H. Mekonnen, T. Haile, M. Ly, Hydrophobic functionalization of cellulose nanocrystals for enhanced corrosion resistance of polyurethane nanocomposite coatings, Appl. Surf. Sci. 540 (2021) 148299. https://doi.org/10.1016/j.apsusc.2020.148299.

[55] L.M. Kalossaka, A.A. Mohammed, G. Sena, L. Barter, C. Myant, 3D printing nanocomposite hydrogels with lattice vascular networks using stereolithography, J. Mater. Res. 36 (2021) 4249–4261. https://doi.org/10.1557/s43578-021-00411-2.

[56] J. Wang, A. Chiappone, I. Roppolo, F. Shao, E. Fantino, M. Lorusso, D. Rentsch, K. Dietliker, C.F. Pirri, H. Grützmacher, All-in-One Cellulose Nanocrystals for 3D Printing of Nanocomposite Hydrogels, Angew. Chemie - Int. Ed. 57 (2018) 2353–2356. https://doi.org/10.1002/anie.201710951.

[57] D. Kam, A. Braner, A. Abouzglo, L. Larush, A. Chiappone, O. Shoseyov, S. Magdassi, 3D Printing of Cellulose Nanocrystal-Loaded Hydrogels through Rapid Fixation by Photopolymerization, Langmuir. 37 (2021) 6451–6458. https://doi.org/10.1021/acs.langmuir.1c00553.

[58] B. Frost, B.P. Sutliff, P. Thayer, M.J. Bortner, E.J. Foster, Gradient poly(Ethylene glycol)

diacrylate and cellulose nanocrystals tissue engineering composite scaffolds via extrusion bioprinting, Front. Bioeng. Biotechnol. 7 (2019) 1–14. https://doi.org/10.3389/fbioe.2019.00280.

[59] Z. Zhang, R. Liu, H. Zepeda, L. Zeng, J. Qiu, S. Wang, 3D Printing Super Strong Hydrogel for Artificial Meniscus, ACS Appl. Polym. Mater. 1 (2019) 2023–2032. https://doi.org/10.1021/acsapm.9b00304.

[60] Y. Fan, Z. Yue, E. Lucarelli, G.G. Wallace, Hybrid Printing Using Cellulose Nanocrystals Reinforced GelMA/HAMA Hydrogels for Improved Structural Integration, Adv. Healthc. Mater. 9 (2020) 1–11. https://doi.org/10.1002/adhm.202001410.

[61] T. Wan, P. Fan, M. Zhang, K. Shi, X. Chen, H. Yang, X. Liu, W. Xu, Y. Zhou, Multiple Crosslinking Hyaluronic Acid Hydrogels with Improved Strength and 3D Printability, ACS Appl. Bio Mater. 5 (2022) 334–343. https://doi.org/10.1021/acsabm.1c01141.

[62] Y. Chen, Y. Liu, J. Ren, W. Yang, E. Shang, K. Ma, L. Zhang, J. Jiang, X. Sun, Conformable core-shell fiber tactile sensor by continuous tubular deposition modeling with water-based sacrificial coaxial writing, Mater. Des. 190 (2020) 108567. https://doi.org/10.1016/j.matdes.2020.108567.

[63] M. Qaim, K.T. Sibhatu, H. Siregar, I. Grass, Environmental, economic, and social consequences of the oil palm boom, Annu. Rev. Resour. Econ. 12 (2020). https://doi.org/10.1146/annurev-resource-110119-024922.

[64] S.A.B. Choiruzzad, A. Tyson, H. Varkkey, The ambiguities of Indonesian Sustainable Palm Oil certification: internal incoherence, governance rescaling and state transformation, Asia Eur. J. 19 (2021). https://doi.org/10.1007/s10308-020-00593-0.

[65] A.L. Ong, C.K. Teh, S. Mayes, F. Massawe, D.R. Appleton, H. Kulaveerasingam, An improved oil palm genome assembly as a valuable resource for crop improvement and comparative genomics in the Arecoideae subfamily, Plants. 9 (2020) 1–15. https://doi.org/10.3390/plants9111476.

[66] A.N. Ashraf, S. Zulkefly, S.M. Adekunle, M.Y. A. Samad, Growth and Biomass yield of Oil Palm (Elaeis guineensis) Seedlings as Influenced by Different Rates of Vermicompost, Eur. J. Eng. Res. Sci. 2 (2017) 17. https://doi.org/10.24018/ejers.2017.2.8.405.

[67] Y. Basiron, C.K. Weng, The Oil Palm and its Sustainability, J. Oil Palm Res. 16 (2004) 1–10.

[68] A.A. Septevani, A. Rifathin, A.A. Sari, Y. Sampora, G.N. Ariani, Sudiyarmanto, D. Sondari, Oil palm empty fruit bunch-based nanocellulose as a super-adsorbent for water remediation, Carbohydr. Polym. 229 (2020) 115433. https://doi.org/10.1016/j.carbpol.2019.115433.

[69] A.A. Septevani, D. Burhani, Y. Sampora, Y.A. Devy, G.N. Ariani, S. Sudirman, D. Sondari, K.N. Mohd Amin, The Effect of Acid Hydrolysis Treatment on the Production of Nanocellulose Based on Oil Palm Empty Fruit Bunches, J. Kim. Terap. Indones. 21 (2019) 31–37. https://doi.org/10.14203/jkti.v21i1.416.

[70] J.Y. Zhu, U.P. Agarwal, P.N. Ciesielski, M.E. Himmel, R. Gao, Y. Deng, M. Morits, M. Österberg, Towards sustainable production and utilization of plant-biomass-based nanomaterials: a review and analysis of recent developments, Biotechnol. Biofuels. 14 (2021). https://doi.org/10.1186/s13068-021-01963-5.

[71] A. Beil, G. Müller, D. Käser, B. Hattendorf, Z. Li, F. Krumeich, A. Rosenthal, V.K. Rana, H. Schönberg, Z. Benkő, H. Grützmacher, Bismesitoylphosphinic Acid (BAPO-OH): A Ligand for Copper Complexes and Four-Electron Photoreductant for the Preparation of Copper Nanomaterials, Angew. Chemie - Int. Ed. 57 (2018) 7697–7702. https://doi.org/10.1002/anie.201800456.

[72] D. Burhani, A.A. Septevani, Isolation of nanocellulose from oil palm empty fruit bunches using strong acid hydrolysis, AIP Conf. Proc. 2024 (2018). https://doi.org/10.1063/1.5064291.

[73] C.A. Xu, M. Lu, K. Wu, J. Shi, Functionalization of nano-cellulose by coupling agent with green strategy, Inorg. Chem. Commun. 134 (2021) 108939. https://doi.org/10.1016/j.inoche.2021.108939.

[74] D. Lee, H. Zhang, S. Ryu, Elastic Modulus Measurement of Hydrogels, (2018) 1–21. https://doi.org/10.1007/978-3-319-76573-0_60-1.

[75] R. Suriano, G. Griffini, M. Chiari, M. Levi, S. Turri, Rheological and mechanical behavior of polyacrylamide hydrogels chemically crosslinked with allyl agarose for two-dimensional gel electrophoresis, J. Mech. Behav. Biomed. Mater. 30 (2014) 339–346. https://doi.org/10.1016/j.jmbbm.2013.12.006.

[76] U.G.T.M. Sampath, Y.C. Ching, C.H. Chuah, R. Singh, P.C. Lin, Preparation and characterization of nanocellulose reinforced semi-interpenetrating polymer network of chitosan hydrogel, Cellulose. 24 (2017) 2215–2228. https://doi.org/10.1007/s10570-017-1251-8.

[77] M. Caprioli, I. Roppolo, S. Magdassi, 3D-printed self-healing hydrogels via Digital Light Processing, Nat. Commun. (n.d.) 1–9. https://doi.org/10.1038/s41467-021-22802-z.

[78] M. Gastaldi, F. Cardano, M. Zanetti, G. Viscardi, C. Barolo, S. Bordiga, S. Magdassi, A. Fin, I. Roppolo, Functional Dyes in Polymeric 3D Printing: Applications and Perspectives, ACS Mater. Lett. (2020). https://doi.org/10.1021/acsmaterialslett.0c00455.

[79] B.K. Nandi, A. Goswami, M.K. Purkait, Adsorption characteristics of brilliant green dye on kaolin, J. Hazard. Mater. 161 (2009). https://doi.org/10.1016/j.jhazmat.2008.03.110.

[80] A. Cosola, M. Sangermano, D. Terenziani, R. Conti, M. Messori, H. Grützmacher, C.F. Pirri, A. Chiappone, DLP 3D – printing of shape memory polymers stabilized by thermoreversible hydrogen bonding interactions, Appl. Mater. Today. 23 (2021). https://doi.org/10.1016/j.apmt.2021.101060.

[81] F. Ganji, S. Vasheghani-Farahani, E. Vasheghani-Farahani, Theoretical description of hydrogel swelling: A review, Iran. Polym. J. (English Ed. 19 (2010) 375–398.

[82] H. Dai, H. Huang, Enhanced swelling and responsive properties of pineapple peel superabsorbent hydrogel by the introduction of carclazyte, 2017. https://doi.org/10.1021/acs.jafc.6b04899.

[83] N. Xia, W. Wan, S. Zhu, Q. Liu, Preparation of crystalline nanocellulose/hydroxypropyl β cyclodextrin/carboxymethyl cellulose polyelectrolyte complexes and their controlled release of neohesperidin-copper (II) in vitro, Int. J. Biol. Macromol. 163 (2020) 1518–1528. https://doi.org/10.1016/j.ijbiomac.2020.07.272.

[84] T. Chen, H. Liu, C. Dong, Y. An, J. Liu, J. Li, X. Li, C. Si, M. Zhang, Synthesis and characterization of temperature/pH dual sensitive hemicellulose-based hydrogels from eucalyptus APMP waste liquor, Carbohydr. Polym. 247 (2020) 116717. https://doi.org/10.1016/j.carbpol.2020.116717.

[85] R. Batmaz, N. Mohammed, M. Zaman, G. Minhas, R.M. Berry, K.C. Tam, Cellulose

nanocrystals as promising adsorbents for the removal of cationic dyes, Cellulose. 21 (2014) 1655–1665. https://doi.org/10.1007/s10570-014-0168-8.

[86] A. Sergeeva, A.S. Vikulina, D. Volodkin, Porous alginate scaffolds assembled using vaterite CaCO3 crystals, Micromachines. 10 (2019) 1–21. https://doi.org/10.3390/mi10060357.

[87] Y. Qin, J. Wang, C. Qiu, X. Xu, Z. Jin, A Dual Cross-Linked Strategy to Construct Moldable Hydrogels with High Stretchability, Good Self-Recovery, and Self-Healing Capability, J. Agric. Food Chem. 67 (2019) 3966–3980. https://doi.org/10.1021/acs.jafc.8b05147.

[88] P. Calvert, Hydrogels for soft machines, Adv. Mater. 21 (2009) 743–756. https://doi.org/10.1002/adma.200800534.

[89] Markets&Markets, Industrial 3D Printing Market with COVID-19 Impact Analysis, by Offering (Printers, Materials, Software, Services), Application, Process, Technology, Industry (Aerospace & Defense, Automotive) and Geography - Global Forecast to 2026, 2022.

[90] M. Shuaib, A. Haleem, S. Kumar, M. Javaid, Impact of 3D Printing on the environment: A literature-based study, Sustain. Oper. Comput. 2 (2021) 57–63. https://doi.org/10.1016/j.susoc.2021.04.001.

[91] M.R. Khosravani, T. Reinicke, 3D-printed sensors: Current progress and future challenges, Sensors Actuators, A Phys. 305 (2020) 111916. https://doi.org/10.1016/j.sna.2020.111916.

[92] J. Nyika, F.M. Mwema, R.M. Mahamood, E.T. Akinlabi, T. Jen, A five-year scientometric analysis of the environmental effects of 3D printing, Adv. Mater. Process. Technol. (2021). https://doi.org/https://doi.org/10.1080/2374068X.2021.1945267.

[93] Markets and Markets, Nanocellulose Market by Type (MFC & NFC, CNC/NCC, and Others), Application (Pulp&paper, composites, biomedical & pharmaceutical, electronics & sensors, and others), Region (Europe, North America, APAC, and Rest of World) - Global Forecast to 2025, 2020.

[94] Markets&Markets, Cellulose Ether & Derivatives Market by Product Type (Methyl Cellulose & Derivatives, Carboxymethyl Cellulose, HEC, HPC, EC), Application (Construction, Pharmaceutical, Personal Care, Food & Beverage), and Region - Global Forecast to 2026, 2022.